Analysis of Clogging Behaviors of Diatomaceous Ceramic Membranes During Membrane Filtration Based upon Specific Deposit

Eiji Iritani, Nobuyuki Katagiri, Tomoaki Tadama, and Hiroaki Sumi
Dept. of Chemical Engineering, Nagoya University, Furo-cho, Chikusa-ku, Nagoya 464-8603, Japan

DOI 10.1002/aic.12111
Published online November 17, 2009 in Wiley InterScience (www.interscience.wiley.com).

Fouling behaviors in membrane filtration of dilute suspension of polystyrene latex (PSL) were examined under constant-pressure conditions using diatomaceous ceramic membranes which are semi-permeable to the PSL. Flux decline behaviors were evaluated in consideration of the effect of the solid permeation through the membrane. The conventional characteristic filtration equation was modified by applying the Kozeny-Carman equation to the filtrate flow through the membrane pores. In the model, the porosity and specific surface area of the membrane were represented by unique functions of the solid deposit retained in the membrane pores. The variations of the filtration rate and filtrate volume with the filtration time were accurately described based upon the modified characteristic filtration equation. It was revealed that the extent of the membrane blocking per unit deposit load increased with the decrease in the pore size of the membrane and with decreasing pressure, but was little influenced by the suspension concentration. © 2009 American Institute of Chemical Engineers *AIChE J,* 56: 1748–1758, 2010

Keywords: solid/liquid separations, membrane filtration, membrane clogging, diatomaceous ceramic membrane, blocking filtration

Introduction

Clarification of very dilute suspensions containing fine particles treated with membranes has been developed specifically to meet the requirement of such water purification processes as ultrapure water production, drinking water treatment, and effluent polishing. In such cases, the particles are captured both in the interior of a porous membrane as well as on its external surface.[1] For this reason, one of the critical issues governing the performance of these filtration processes may be a significant decay in flow rate for constant-pressure operation caused by clogging phenomena of membrane pores arising from particles reaching the membrane.

The blocking filtration model proposed by Hermans and Bredée[2,3] and subsequently systematized by Grace,[4] Shirato et al.,[5] Hermia,[6] and Iritani et al.[7] has been exclusively used in the analysis of the clogging behaviors of membranes during membrane filtration.[8–11] For constant-pressure filtration, four different kinds of filtration modes were compiled into a common differential equation with two constants, n_v and k_v.

$$\frac{d^2\theta}{dv^2} = k_v\left(\frac{d\theta}{dv}\right)^{n_v}, \tag{1}$$

where θ is the filtration time, v is the cumulative filtrate volume per unit effective cross-sectional membrane area, n_v is the blocking index depending upon the filtration mode, and k_v

Correspondence concerning this article should be addressed to E. Iritani at iritani@nuce.nagoya-u.ac.jp.

is the resistance coefficient. The value of n_v is 2, 1.5, 1, and 0 for complete blocking, standard blocking (pore constriction), intermediate blocking, and cake mode of filtration, respectively, and thus the possible n_v-values are restricted. Recently, several combined models have been developed that used two-staged mechanisms to describe membrane fouling.[12–16] Bowen et al.[17] and Iritani et al.,[18] almost at the same time, suggested that the value of n_v in Eq. 1 varied successively during the course of filtration in dead-end microfiltration of bovine serum albumin solutions. More recently, Hwang et al.[19] also observed a similar behavior in particulate microfiltration. Iritani et al.[20] derived the same differential equation as Eq. 1 by accounting for the variations of both the porosity and specific surface area of the membrane during filtration in the Kozeny-Carman equation. As a result, it was revealed that Eq. 1 may be applicable to an arbitrary n_v-value and stems from a single fouling mechanism. Bolton et al.[21] also focused attention on the Kozeny-Carman equation to develop a fiber-coating model, in which the fibrous filter becomes plugged as solids coated the surfaces of fibers.

In each instance, it is implicitly assumed that all solids filtered are retained by the membrane. If not, the solids deposited inside the membrane must be directly proportional to the filtrate volume to assure the validity of Eq. 1. However, in practice, there exists some solid leakage through the membrane, and the sieving coefficient of the solids varies with a concomitant decline in the flux during the course of filtration. In depth filtration conducted using a sand filter, the pressure drop across the granular bed under the constant-rate condition has been generally related to the solid uptake in the pores.[22–24] Therefore, also in clarification filtration using the membrane, the flux decline behaviors under the constant-pressure condition should be analyzed taking into account the solid uptake in the interior of the membrane or filter cake.[25–27] Although the application of the ingenious depth filtration approach to standard blocking filtration law has been recently introduced to analyze the flux decline behaviors in membrane filtration, the experimental verification of the model presented remains insufficient.[28] Moreover, the mainstay of the models describing the clogging behaviors of membranes currently continues to center around the blocking filtration model because of the simplicity of the model.

In the present article, the behaviors of flux decline and solid permeation in membrane filtration of monodisperse polystyrene latex (PSL) are examined under the constant-pressure condition using diatomaceous ceramic membranes from an experimental viewpoint. From the practical standpoint, a modified blocking filtration model is presented as a simplified model for describing the flux decline behaviors in consideration of the solid uptake in the membrane pores. The effects of the average porosity (or pore size) of the membrane, the applied filtration pressure, and the suspension concentration on the flux decline behaviors are quantified based upon the model presented.

Experimental

Materials

The particles employed in the experiments were monodisperse PSL with a particle diameter of 0.522 μm (variation within $\pm$0.089 μm) (Dow Chemical Japan), whose true density was 1060 kg/m^3. The particles were suspended in ultrapure water prepared with an ultrapure water system for laboratory use (Puric-R, Organo). The mass fraction s of solids in the suspension ranged from 1×10^{-6} to 1×10^{-5}.

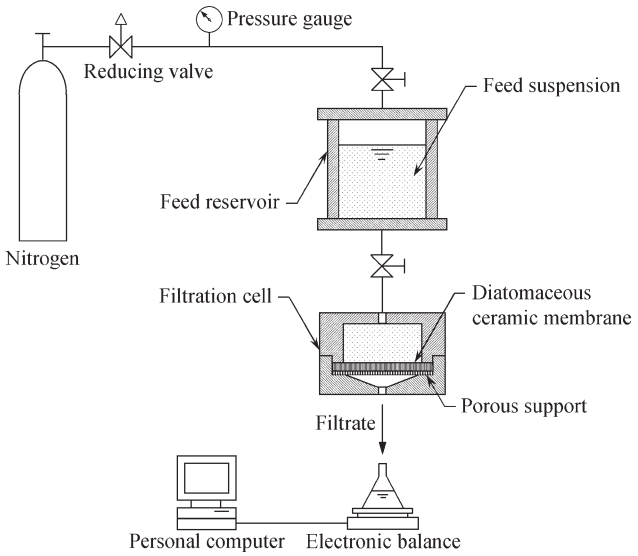

Figure 1. Schematic diagram of experimental apparatus.

Diatomaceous ceramic membranes of 4.7-mm thickness and 25.0-mm diameter with a symmetric structure having various porosities, kindly supplied by Showa Chemical Industry, were used for all experiments. According to the manufacturer's report, the membranes were produced by sintering the compact of the diatomaceous filter aids, Radiolite #700 (Showa Chemical Industry), and the porosity of the membrane was varied by changing the molding pressure. The porosity of the membrane was calculated from the measurements of the bulk volume and the weight of the membrane using the value of the true density of the membrane material. The true density of the powder obtained by pounding the membrane in a mortar was measured by the pycnometer and was calculated to be 2350 kg/m^3. It was used as the true density of the membrane material. The pore size distribution of the membrane was measured with a mercury intrusion porosimeter.

Experimental apparatus and technique

A schematic diagram of the experimental apparatus for membrane filtration is illustrated in Figure 1. A self-produced, unstirred batch filtration cell with an effective membrane area of 3.14 cm^2 was used in this research. The filtration cell consisted essentially of a stainless steel cylindrical vessel, equipped with a porous support on which the diatomaceous ceramic membrane was placed.

Dead-end membrane filtration experiments were performed under conditions of constant pressure ranging from 98 to 392 kPa controlled by a reducing valve by applying compressed nitrogen gas after the PSL suspension was introduced into both the filtration cell and the acrylic feed suspension reservoir. The filtrate was collected in a filtrate

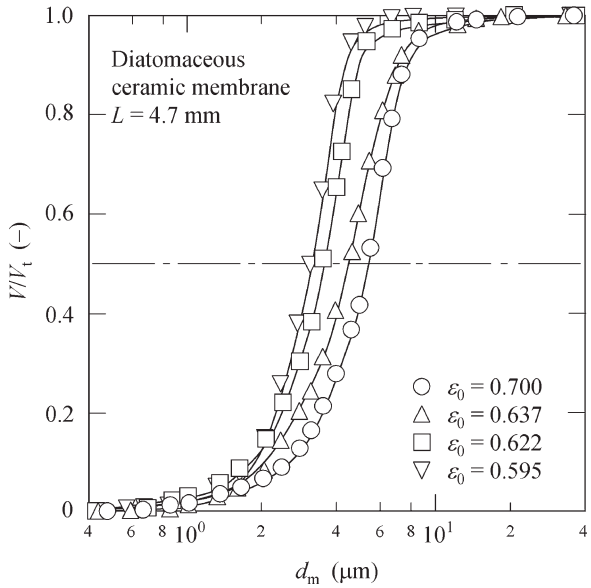

Figure 2. Pore size distributions of membranes with different porosities.

reservoir placed on an electric balance connected to a personal computer to collect and record the filtrate mass vs. filtration time data. The weights were converted to volumes using filtrate density correlations. The filtrate reservoir was replaced every increment of the filtrate volume ranging from 400 to 1000 cm^3, to sample the filtrate and measure the PSL concentration in the filtrate. As a result, it is possible to depict the plot of PSL concentration in the filtrate vs. the filtrate volume per unit membrane area at good intervals. The PSL concentration in the filtrate and the bulk suspension was measured spectrophotometrically by reading the absorbance at a wavelength of 306 nm by using the depletion method and a specific calibration curve obtained with PSL suspensions of known concentrations. Most filtration experiments were performed in twice and showed good reproducibility with the errors within several percent.

Prior to the filtration test, the hydraulic permeability of the membrane itself was determined by permeating the pure water through the membrane under conditions of various pressures.

To obtain the average specific filtration resistance α_{av} of the filter cake, dead-end microfiltration experiments were also performed using mixed cellulose ester microfiltration membranes (Millipore) with a nominal pore size of 0.45 μm, making it essentially impermeable to PSL particles used in this research.

Results and Discussion

Pore size of membrane

The pore size distributions of membranes measured by using a mercury intrusion porosimeter are shown in Figure 2, where V is the total volume of pores smaller than an arbitrary diameter d_m, and V_t is the total volume of all pores. In the figure, the data are plotted for the membranes with the different porosities ε_0 obtained by changing the molding pressure in the manufacturing process of membranes. As the porosity decreases, the pore size distribution tends to shift to smaller values. This suggests that the pore size of the membrane is changed by the control of the porosity of the membrane. Although the pore size shows relatively broad distributions, the median size falls within the range of 3 to 6 μm in each instance. Since the size of PSL employed in this research is one order of magnitude less than the pore size of the membrane, it is anticipated that filtration of dilute suspension is governed by the mechanism of depth filtration.

In Figure 3, the average diameter $d_{m,av}$ of the pores of the membrane is plotted against the porosity ε_0 of the membrane. The median size of the pores determined from Figure 2 is compared with the equivalent diameter of the pores evaluated from the pure water permeation test. The Kozeny-Carman equation for describing the flow through a porous medium is written as

$$u = \frac{\varepsilon_0^3}{k_0 S_0^2 (1-\varepsilon_0)^2} \cdot \frac{p}{\mu L}, \tag{2}$$

where u is the permeation rate of water through the membrane, S_0 is the effective specific surface area of the membrane, p is the applied pressure, μ is the viscosity of permeate, L is the effective thickness of the membrane, and k_0 is the Kozeny constant, which can be approximated by the value of 5.0 for granular beds of particles of irregular shape.[29] On the basis of the concept of the hydraulic radius that is very useful for nondescript geometry, the equivalent diameter $d_{m,av}$ is related to both the specific surface area S_0 and porosity ε_0 by

$$d_{m,av} = \frac{4\varepsilon_0}{S_0(1-\varepsilon_0)}. \tag{3}$$

The specific surface area S_0 is eliminated between Eqs. 2 and 3 to give

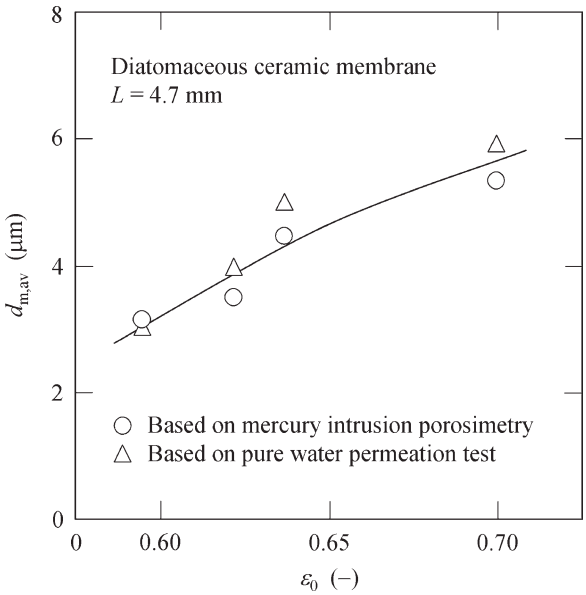

Figure 3. Relation between average diameter $d_{m,av}$ of pores of membrane and intrinsic porosity ε_0 of membrane.

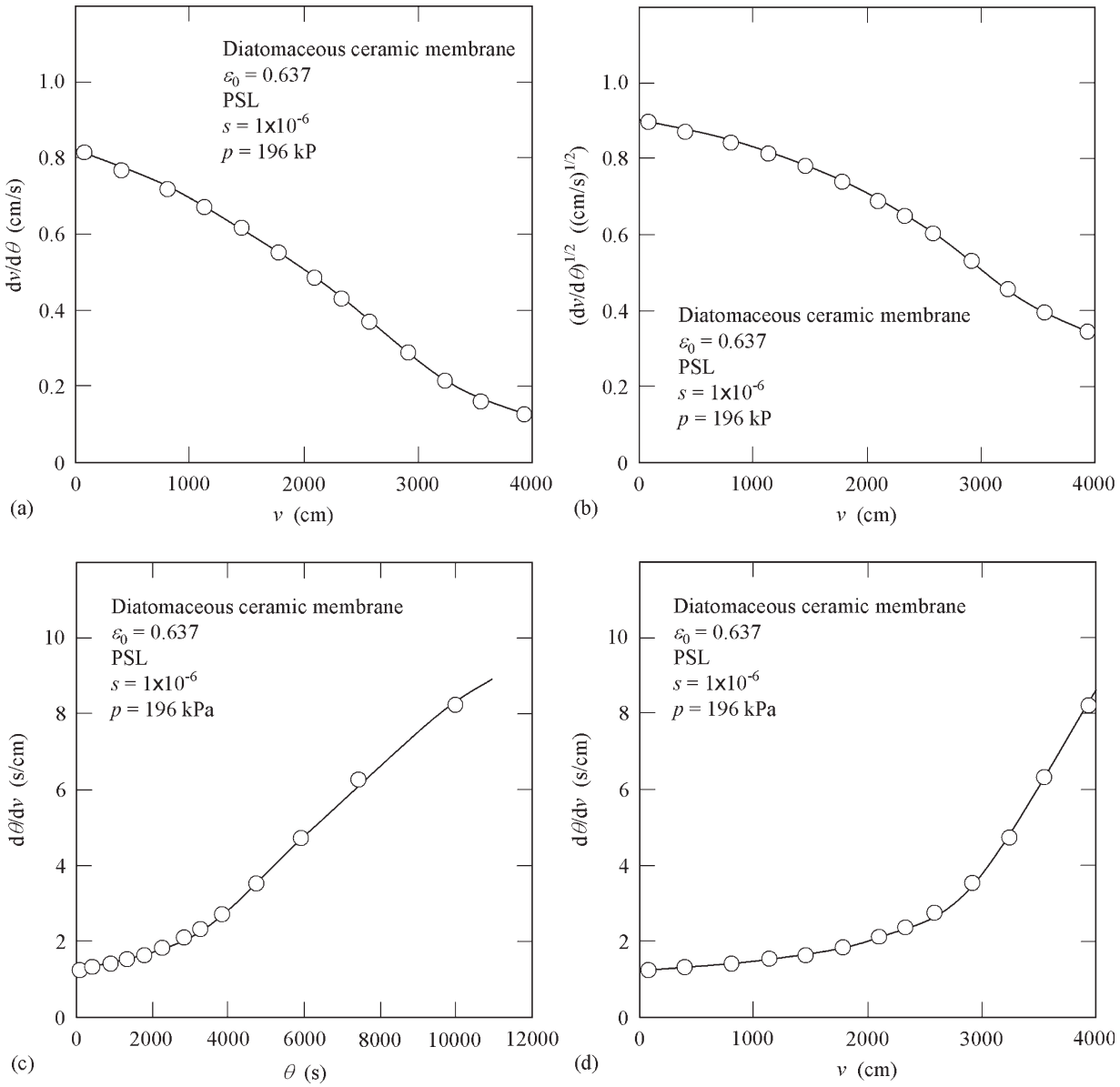

Figure 4. Four types of plots concerning blocking filtration laws.

(a) $dv/d\theta$ vs. v; (b) $(dv/d\theta)^{1/2}$ vs. v; (c) $d\theta/dv$ vs. θ; (d) $d\theta/dv$ vs. v.

$$d_{\mathrm{m,av}} = 4\left(\frac{\mu k_0 L u}{\varepsilon_0 p}\right)^{1/2}. \tag{4}$$

Thus, from Eq. 4 it is possible to calculate the equivalent diameter $d_{\mathrm{m,av}}$ by use of the measurements of the water permeation rate u. It can be seen from the figure that the equivalent diameter evaluated from the hydraulic permeability is in fairly good agreement with the median size of pores measured by the mercury intrusion porosimeter. Consequently, the conclusion is reached that the average pore size is well evaluated from the water permeation test. It should be noted that the diatomaceous ceramic membranes show relatively high porosities ranging from 0.6 to 0.7 among inorganic membranes. This may be attributed to the high porous structure of the diatomaceous earth used as the raw materials of the membrane.

Results and discussion based upon classical approach

Four types of plots of $dv/d\theta$ vs. v, $(dv/d\theta)^{1/2}$ vs. v, $d\theta/dv$ vs. θ, and $d\theta/dv$ vs. v are shown for the membrane with the porosity ε_0 of 0.637 in Figure 4, based upon the raw filtration data of the cumulative filtrate volume v collected per unit effective membrane area vs. the filtration time θ. If the filtration mechanism is controlled by the complete blocking law corresponding to $n_v = 2$ in Eq. 1, then the plots of $dv/d\theta$ vs. v should show a linear fit. However, there is a definite curvature in the plots on the whole as shown in Figure 4a, and hence the complete blocking law cannot be applied to explain the flux decline behaviors during filtration. Similarly, plots of $(dv/d\theta)^{1/2}$ vs. v in Figure 4b for the standard blocking law ($n_v = 1.5$ in Eq. 1), $d\theta/dv$ vs. θ in Figure 4c for the intermediate blocking law ($n_v = 1$), and $d\theta/dv$ vs. v in

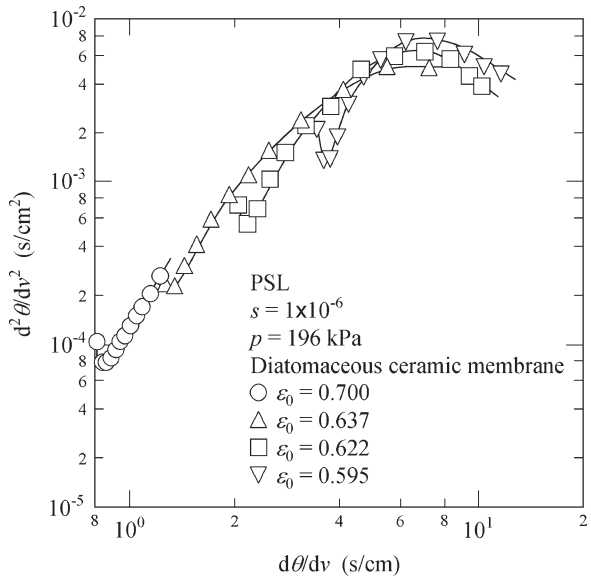

Figure 5. Logarithmic plots of $d^2\theta/dv^2$ vs. $d\theta/dv$.

Figure 4d for the mode of cake filtration ($n_v = 0$) are also found to be nonlinear. It is of interest to note that the experimental data over the course of depth filtration cannot be expressed by only a single blocking filtration law. Therefore, these plots are inconvenient for data analysis and model identification. Thus, according to the conventional analysis, it must be concluded that the governing filtration mechanism gradually changes with the progress of filtration.[17–19] Only for a short-term experiment may the experimental data be elucidated by a single blocking filtration law. This situation is similar to results in the data analysis of the previous investigators,[30–32] who have employed only a single blocking filtration law. The plots of $d\theta/dv$ vs. v for cake filtration represent the increase-resistance behavior to flow during the filtration process. It can be seen from the figure that the filtration resistance increases markedly due to the internal deposition compared with the initial membrane resistance expected from the value of $d\theta/dv$ at the commencement of filtration, as filtration proceeds.

The logarithmic plots of $d^2\theta/dv^2$ vs. $d\theta/dv$ corresponding to Eq. 1 for a variety of membranes with different initial porosities ε_0 are shown in Figure 5 as the characteristic filtration curve of the blocking filtration law. In the calculation, the term ($d^2\theta/dv^2$) can be evaluated by the stepwise difference quotient of the raw data of the reciprocal filtration rate ($d\theta/dv$) vs. the filtrate volume v per unit membrane area, for instance, as shown in Figure 4d. Therefore, there is some scatter in the results due to the stepwise differentiation of the raw data. The plots in each run show a convex curve with the exception of the case when porosity is 0.7. The slope of the curve gradually decreases with the increase of $d\theta/dv$ in accordance with the progress of filtration. This means that the filtration behavior during depth filtration cannot be described by only a single blocking filtration law.

Variation of particle retention by membrane with time

Spectrophotometric analysis of filtrate samples affords the data of the solid uptake in the porous structure of the membrane. Figure 6 shows the observed rejection R with PSL plotted as a function of the filtrate volume v per unit effective membrane area, for the experimental runs described in Figure 5. The rejection R is defined as

$$R = 1 - \frac{c}{s}, \tag{5}$$

where c and s are the mass fraction of PSL particles in the filtrate and the bulk suspension, respectively. A relatively high rejection at the onset of filtration may be attributed to the adsorption of PSL particles within the microporous structure of the membrane. Thereafter, the rejection R increases remarkably with the progress of filtration. This can be expected because the pore size decreases steadily owing to the particle deposition inside a porous membrane, leading to the improvement in the ability to capture the particles. This trend becomes pronounced with the decrease in the initial porosity ε_0 of the membrane used, which is associated with the decrease in the initial pore size $d_{m,av}$ of the membrane. Therefore, there is a distinct dip of rejection at the initial stage of filtration for the cases of $\varepsilon_0 = 0.622$ and 0.595. Almost perfect rejection was eventually attained up to porosities as high as 0.637.

When particles are far smaller than the size of pores of a membrane, the flux decline may be caused by the deposition of particles trapped within the internal structure of the membrane. In other word, as particles are deposited, the pores become constricted, thereby significantly reducing the permeability of the membrane. Therefore, the flux decline behavior must be analyzed in view of the variation with

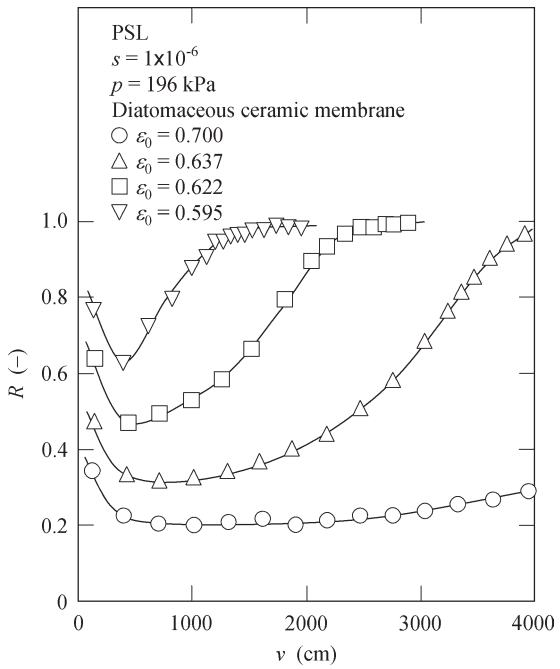

Figure 6. Variation of rejection R of membrane with filtrate volume v per unit effective membrane area.

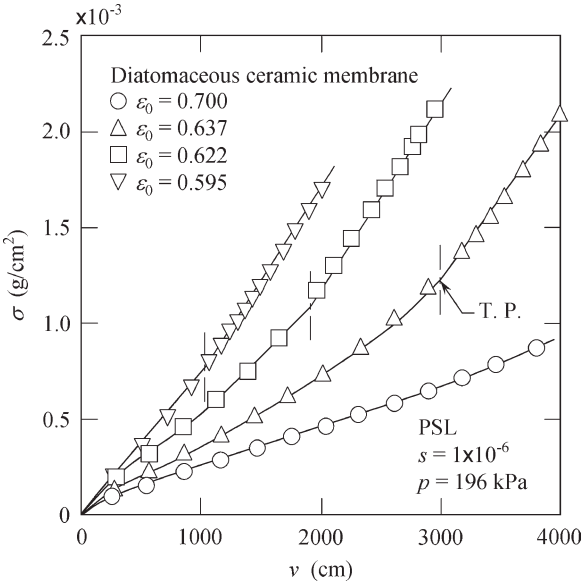

Figure 7. Variation of specific deposit σ with filtrate volume v per unit effective membrane area.

time of the particle accumulation within the pores of the membrane. The mass σ of particles accumulated within the pores per unit membrane area referred to as the specific deposit is related to the rejection R by

$$\sigma = \frac{\rho_s}{\rho_s - (\rho_s + \rho e_p)s} \int_0^w Rsdw, \tag{6}$$

where ρ_s is the density of solids, ρ is the density of the liquid, e_p is the void ratio of the assemblages of the solid particles accumulated within the pores, and w is the filtrate mass per unit effective membrane area. As a satisfactory approximation for very dilute suspension where s ranges from 1×10^{-6} to 1×10^{-5} in this investigation, Eq. 6 may be simplified by

$$\sigma = \int_0^w Rsdw. \tag{7}$$

In Figure 7, the specific deposit σ calculated from Eq. 7 by using the rejection data shown in Figure 6 is plotted against the filtrate volume v per unit effective membrane area. It is indicated that the lower porosity of the membrane produces more severe clogging of particles. The specific deposit σ varies nonlinearly with the filtrate volume v for the experimental runs described in Figure 5 as a consequence of the variation of the rejection R with time. The rate of increase of the specific deposit with respect to v generally increases with the increase in v. As the filtration process continues, the plots approach a straight line with the slope of ρs closely in accordance with the material balance of cake filtration approximated by

$$d\sigma = sdw = \rho sdv. \tag{8}$$

This clearly indicates that all the particles filtered are retained by the membrane during the course of cake filtration in accord with common knowledge. It should be noted that the distinct breakthrough of particles in effluent was not observed at the transient stage of depth to cake filtration.

Results and discussion based upon newly developed approach

In the previous paper,[20] a theoretical background of the characteristic filtration Eq. 1 was developed in consideration of the variation of the porosity ε and specific surface area S of the membrane during filtration in the Kozeny-Carman equation represented by

$$\frac{dv}{d\theta} = \frac{\varepsilon^3}{k_0 S^2 (1-\varepsilon)^2} \cdot \frac{p}{\mu L}, \tag{9}$$

where ε and S are described by Ref. 20.

$$\varepsilon = \varepsilon_0 - K_v v = \left(1 - \frac{K_v v}{\varepsilon_0}\right)\varepsilon_0, \tag{10}$$

$$S^2(1-\varepsilon)^2 = \left(1 - \frac{K_v v}{\varepsilon_0}\right)^{\beta} S_0^2 (1-\varepsilon_0)^2. \tag{11}$$

The coefficient K_v represents the bulk volume of the layer of particles deposited inside a porous membrane caused by unit filtrate volume per unit effective membrane area. Note that the term K_v appearing in Eqs. 10 and 11 is identical to the term K used in the previous article.[20] The power index β in Eq. 11 is a constant depending upon the mode of the morphology of the deposit assemblages, and it is identical to the index β used in the previous article.[20] The index β is defined by Ref. 20.

$$\frac{D_s}{D_{s0}} = \left(\frac{D}{D_0}\right)^{\beta}, \tag{12}$$

where D_s is the representative diameter of pores on a wetted perimeter basis, D is the representative diameter of pores on a flow cross-sectional area basis, and the subscript 0 indicates the value of the clean membrane. Substituting Eqs. 10 and 11 into Eq. 9 and differentiating the result with respect to the filtrate volume v, Eq. 1 was derived, as shown in more detail elsewhere.[20] However, Eq. 1 is not satisfactory as it was implicitly assumed in the analysis that the amount of the particle accumulation within the pores of the membrane varies linearly with the filtrate volume.

In this article, the general framework underlying the model presented in the previous paper[20] is extended to account for the variation with time of the amount of the particle accumulation within the pores of the membrane. Replacing the filtrate volume v in Eqs. 10 and 11 by the specific deposit σ, one obtains

$$\varepsilon = \varepsilon_0 - K\sigma = \left(1 - \frac{K\sigma}{\varepsilon_0}\right)\varepsilon_0, \tag{13}$$

$$S^2(1-\varepsilon)^2 = \left(1 - \frac{K\sigma}{\varepsilon_0}\right)^{\beta} S_0^2 (1-\varepsilon_0)^2, \tag{14}$$

where K is the bulk volume of the layer of particles deposited inside a porous membrane caused by unit specific deposit.

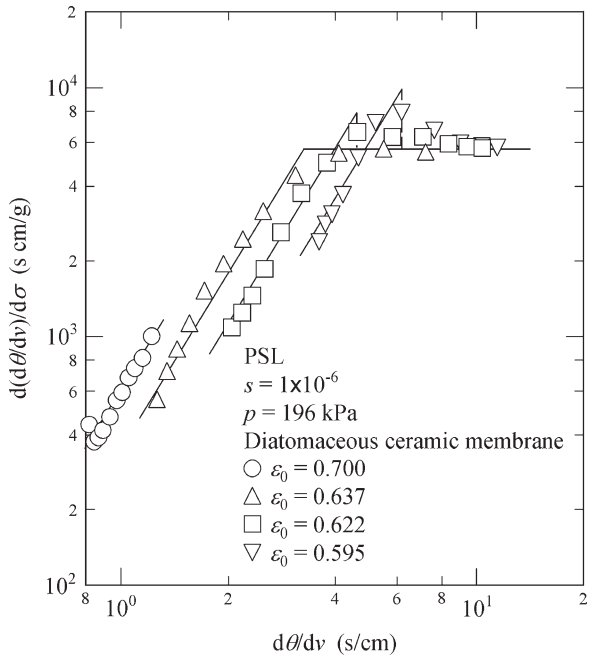

Figure 8. Logarithmic plots of $d(d\theta/dv)/d\sigma$ vs. $d\theta/dv$.

Note that the power index β in Eq. 14 is identical to β in Eqs. 11 and 12. Substituting Eqs. 13 and 14 into Eq. 9, one obtains

$$\frac{d\theta}{dv} = (1 + N\sigma)^M \left(\frac{d\theta}{dv}\right)_0, \tag{15}$$

where $M = \beta - 3$, $N = -K/\varepsilon_0$, and $(d\theta/dv)_0$ is the initial reciprocal filtration rate corresponding to the hydraulic resistance of the membrane itself. Differentiating Eq. 15 with respect to the specific deposit σ, the modified form of the characteristic filtration Eq. 1 is expressed as

$$\frac{d(d\theta/dv)}{d\sigma} = k\left(\frac{d\theta}{dv}\right)^n, \tag{16}$$

where k $(=MN(d\theta/dv)_0^{1/M} = (3 - \beta)K(d\theta/dv)_0^{1/(\beta-3)}/\varepsilon_0)$ is the resistance constant of the specific deposit basis, and n $[=(M - 1)/M = (\beta - 4)/(\beta - 3)]$ is the blocking index.

If the correlation of the specific deposit σ and the filtrate volume v is experimentally obtained, then the derivative $d(d\theta/dv)/d\sigma$ may be calculated from the stepwise difference quotient using the raw data of $d\theta/dv$ vs. v. The logarithmic plots of $d(d\theta/dv)/d\sigma$ vs. $d\theta/dv$ calculated by utilizing the data of the solid uptake in Figure 7 are shown in Figure 8 as the newly developed characteristic filtration curve. Of particular interest, when comparing the data shown in Figures 5 and 8 is the shapes of the curves. For each porosity, the plots in Figure 8 show a linear relation with the same slope of 2.35 in accord with Eq. 16 except for the last part of filtration, in sharp contrast to the results shown in Figure 5. For instance, the data for the porosity ε_0 of 0.595 shown in Figure 8 show a very strong linear relationship (the coefficient of determination $R^2 > 0.99$). In contrast, the R^2 value drops to 0.81 when the data are plotted in the manner shown in Figure 5. Thus, Eq. 16 provides a much better description of depth filtration behaviors than Eq. 1. The value of K in Eqs. 13 and 14 is determined from the logarithmic plots of $d(d\theta/dv)/d\sigma$ vs. $d\theta/dv$ based upon Eq. 16, and it ranges from 389 to 532 m^2/kg.

Once the limiting capacity of pores has been reached due to deposition of particles over a long time, the formation of a filter cake on the membrane surface occurs, and consequently the particles accumulate on the surface of the permeable cake. For the case where filtration is cake-controlled, the value of n drops to zero toward the end of the curve after the transitory period[19,33] as indicated in the figure, and then Eq. 16 reduces to

$$\frac{d(d\theta/dv)}{d\sigma} = k_c, \tag{17}$$

where k_c is the value of $d(d\theta/dv)/d\sigma$ during the cake filtration period and is indicative of the specific filtration resistance of constant-pressure cake filtration. The value of k_c obtained from the horizontal line in the figure is 5.6×10^3 s cm/g, and it is roughly comparable with the value of 5.1×10^3 s cm/g determined from the dead-end microfiltration experiment conducted using the retentive microfiltration membrane with the pore size of 0.45 μm. The value of $d\theta/dv$ at the critical point making the transition from depth to cake filtration depends upon the porosity of the membrane, and it is determined from the linearity of the plots of σ vs. v during the cake filtration period. As shown in Figure 7, the specific deposit σ_t at the transition point (shown as T. P. in the figure) increases with the increasing porosity of the membrane. It was also clarified that the deposited solid volume at the transition point was considerably smaller than the initial pore volume of the membrane. For instance, the percent ratio is 0.239 percent in the case of the initial porosity of 0.595.

In Figure 9, the filtration rate $(dv/d\theta)$ is plotted against the filtrate volume v per unit effective membrane area for membranes with different initial porosities ε_0. The solid

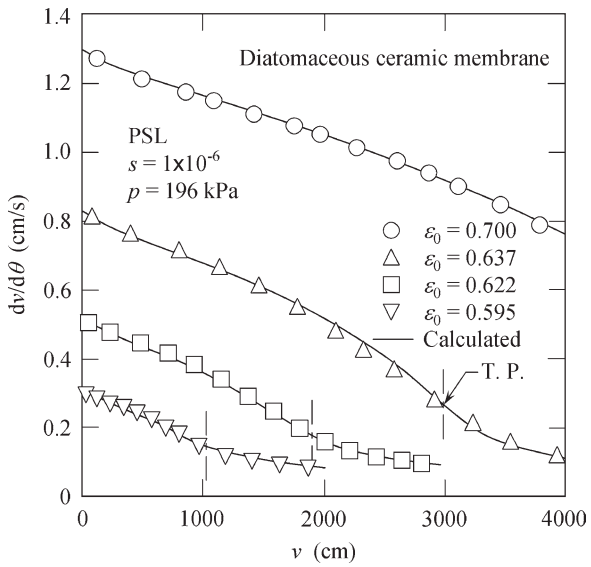

Figure 9. Relation between filtration rate $(dv/d\theta)$ and filtrate volume v per unit effective membrane area.

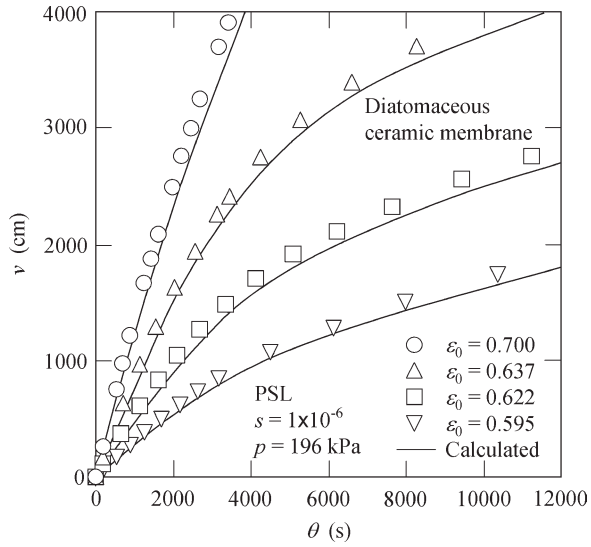

Figure 10. Variation of filtrate volume v with filtration time θ.

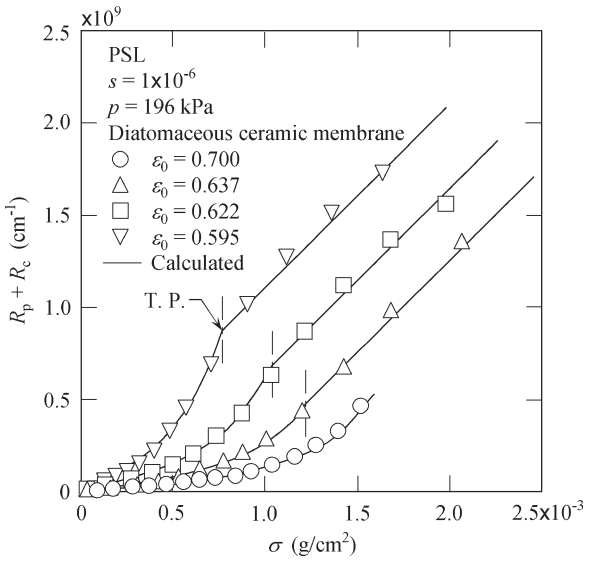

Figure 11. Relation between filtration resistance (R_p + R_c) and specific deposit σ.

curves on this figure during blocking filtration are the calculations obtained based upon Eq. 15 and the relation between σ and v shown in Figure 7, using the initial value of the reciprocal filtration rate, $(d\theta/dv)_0$, and the values of k and n. The values of k and n are determined with the use of Eq. 16 from the straight lines in Figure 8. The transition point from blocking to cake filtration was determined from the onset of linearity of the plots shown in Figure 7, and the flux decline behaviors during cake filtration were evaluated with the aid of the value of k_c determined from the data of the cake filtration experiment conducted using the retentive microfiltration membrane. The calculations are in excellent agreement with the experimental data throughout the course of filtration.

To evaluate the variation of the filtrate volume v with time during blocking filtration, Eq. 15 can be integrated by numerical methods, using the relation between σ and v shown in Figure 7. In Figure 10, the experimental data shown in Figure 9 are replotted in the form of the volume v filtered vs. the filtration time θ. The experimental data are compared with the calculations during blocking and cake filtration, good agreement being observed.

Based upon the resistance-in-series model in filtration developed from Darcy's law,[34] the filtration rate $(dv/d\theta)$ is given by

$$\frac{dv}{d\theta} = \frac{p}{\mu R_t} = \frac{p}{\mu\left(R_m + R_p + R_c\right)}, \tag{18}$$

where R_t is the overall filtration resistance, R_m $(= p(d\theta/dv)_0/\mu)$ is the intrinsic resistance of the membrane, R_p is the resistance of the membrane clogging and R_c is the resistance arising from the cake formation. In general, the increase in the filtration resistance during filtration is brought about by the capture of the particles inside a porous membrane, or on its surface. On the condition that the cake resistance R_c is negligible in the period where the membrane blocking dominates, Eq. 15 can be substituted into Eq. 18 to obtain

$$R_p = \left\{(1 + N\sigma)^M - 1\right\}R_m \quad \sigma \le \sigma_t. \tag{19}$$

In the subsequent cake filtration period, the resistance $(R_p + R_c)$ added by the specific deposit σ can be given by

$$R_p + R_c = \left\{(1 + N\sigma_t)^M - 1\right\}R_m + \alpha_{av}(\sigma - \sigma_t) \quad \sigma \ge \sigma_t, \tag{20}$$

where α_{av} represents the average specific filtration resistance of the filter cake deposited on the membrane surface.[35]

In Figure 11, the resistance $(R_p + R_c)$ is plotted against the specific deposit σ. The solid curves represent the

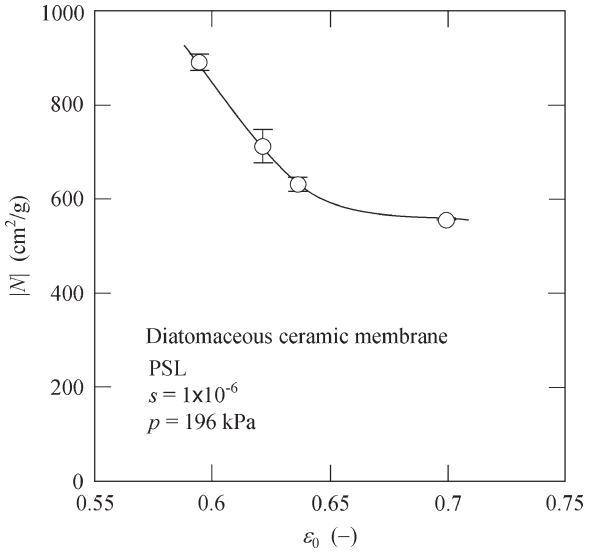

Figure 12. Effect of porosity of membrane on coefficient $|N|$ for specific deposit σ in Eq. 15.

The error bars represent the 95% confidential interval.

calculations obtained using Eqs. 19 and 20. The value of α_{av} used in the calculations is determined from the cake filtration experiment conducted using the retentive microfiltration membrane with the pore size of 0.45 μm. The calculations compare favorably with the experimental data. The curve is concave upward during the blocking filtration period, and thus the increase in the clogging resistance becomes pronounced with the progress of filtration. Subsequently, in the cake filtration period, the resistance increases in direct proportion to the specific deposit σ, and the proportional constant corresponds to the average specific filtration resistance α_{av} of the filter cake.

The effect of the porosity ε_0 of membranes on the coefficient $|N|$ for the specific deposit σ appearing in Eq. 15 is shown in Figure 12, in which the absolute value of N is used to avoid a negative sign. The term $|N|$ $(=K/\varepsilon_0)$ indicates a measure of the degree of the membrane blockage per unit deposit load, and it increases with lower porosity of membranes, probably because of not only the decrease of ε_0 but also the increase of K in the term $|N|$. It can be, therefore, concluded that the lower porosity is responsible for more severe blocking of the membrane.

Figure 13 describes the dependence of the applied filtration pressure p on the coefficient $|N|$. The increase in the pressure p causes the coefficient $|N|$ to be lower, and thus the membrane fouling per unit specific deposit becomes moderate as the pressure p increases. The possible reason is that the value of K appearing in the definition of $|N|$ decreases with increasing pressure because of the deposit assemblages with denser structure formed under higher pressure.

The effect of the suspension concentration s on the coefficient $|N|$ is shown in Figure 14. Experimental data clearly suggest that the coefficient $|N|$ is relatively independent of

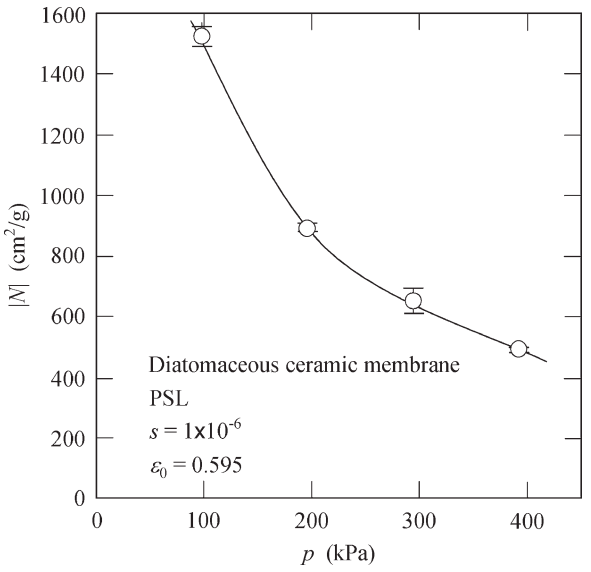

Figure 13. Effect of applied filtration pressure p on coefficient $|N|$ for specific deposit σ in Eq. 15.

The error bars represent the 95% confidential interval.

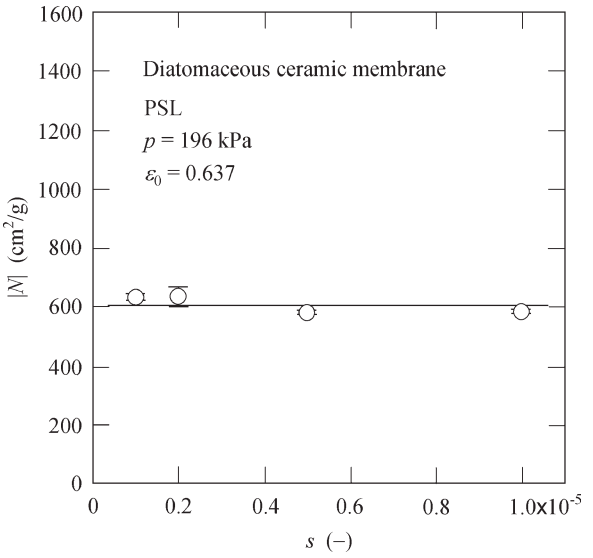

Figure 14. Effect of suspension concentration s on coefficient $|N|$ for specific deposit σ in Eq. 15.

The error bars represent the 95% confidential interval.

the suspension concentration s. It can be inferred that the extent of the membrane fouling is little influenced by the suspension concentration s the specific deposit σ being equal.

In this article, the single-component system of PSL was tested to validate the model presented. As the next step, it becomes extremely important to extend the range of application of the model into the actual complicated foulants. As the rejection R (or the specific deposit σ) is largely influenced by the particle size, we believe that the model considering the specific deposit in the analysis of flux decline behaviors will be also of considerable benefit for the description of filtration behaviors of the polydisperse particle mixture. As the future issue, it will be necessary to carry out the experiments using the mixture of PSL. It would appear that the results obtained by particle mixture experiments provide new insight into the refinement of the model.

Conclusions

The behaviors of flux decline and solid permeation in constant-pressure membrane filtration of very dilute suspensions were examined by a combination of PSL suspensions and the semi-permeable, diatomaceous ceramic membranes, varying porosities of the membrane, filtration pressures, and suspension concentrations. The modified characteristic filtration equation describing the rate of change in the filtration resistance of the clogged semi-permeable membrane was afforded by accounting for the variations of both the porosity and specific surface area of the membrane caused by the capture of the solids within the membrane pore structure in Kozeny-Carman equation, through the introduction of the specific deposit. The variations of the filtration rate and filtrate volume with the filtration time were adequately described based

upon the modified characteristic filtration equation. As a result, it was clarified that the gradual decrease in the filtration flux rate with time occurred due to the capture of solid particles onto the surfaces of pores in the membrane. For depth filtration examined in this paper, it was also shown that the extent of the membrane blocking per unit deposit load increased with the decreasing porosity (leading to the decrease in the pore size) of the membrane and with decreasing filtration pressure, while it was unaffected by the suspension concentration. Future studies using the mixture of PSL will be needed to apply the model to more complicated systems.

Acknowledgments

This work has been partially supported by a Grant-in-Aid for Scientific Research from the Ministry of Education, Culture, Sports, Science and Technology, Japan. The authors acknowledge with sincere gratitude the financial support leading to the publication of this article. The authors also express their sincere appreciation to Showa Chemical Industry for their generous contribution of the diatomaceous ceramic membranes employed in this research.

Notation

c = mass fraction of solids in filtrate
D = representative diameter of pores of flow cross-sectional area basis, m
D_s = representative diameter of pores of wetted perimeter basis, m
d_m = pore size of membrane, m
$d_{m,av}$ = average diameter of pore of membrane, m
e_p = void ratio of assemblages of solids accumulated within pores
K = bulk volume of layer of particles deposited inside porous membrane caused by unit specific deposit, m^2/kg
K_v = bulk volume of layer of particles deposited inside porous membrane caused by unit filtrate volume per unit effective membrane area, m^{-1}
k = constant in Eq. 16, $kg^{-1}\ m^{n+1}\ s^{1-n}$
k_0 = Kozeny constant
k_c = specific filtration resistance of constant-pressure cake filtration in Eq. 17, m s/kg
k_v = constant in Eq. 1, $m^{n-2}\ s^{1-n}$
L = effective thickness of membrane, m
M = constant in Eq. 15
N = constant in Eq. 15, m^2/kg
n = constant in Eq. 16
n_v = constant in Eq. 1
p = applied pressure, Pa
R = rejection
R_c = cake resistance, m^{-1}
R_m = intrinsic resistance of membrane, m^{-1}
R_p = resistance of membrane clogging, m^{-1}
R_t = overall filtration resistance, m^{-1}
S = specific surface area of membrane, m^{-1}
s = mass fraction of solids in bulk suspension
u = permeation rate of water through membrane, m/s
V = total volume of pores smaller than diameter d_m, m^3
V_t = total volume of all pores, m^3
v = cumulative filtrate volume per unit effective membrane area, m^3/m^2
w = filtrate mass per unit effective membrane area, kg/m^2

Greek letters

α_{av} = average specific filtration resistance of filter cake, m/kg
β = constant in Eq. 11
ε = porosity of membrane
θ = filtration time, s
μ = viscosity of permeate, Pa s
ρ = density of liquid, kg/m^3
ρ_s = density of solids, kg/m^3
σ = specific deposit, kg/m^2

Subscripts

0 = initial value
t = value at transition

Literature Cited

1. Ohn T, Jami MS, Iritani E, Mukai Y, Katagiri N. Filtration behaviors in constant rate microfiltration with cyclic backwashing of coagulated sewage secondary effluent. *Sep Sci Technol*. 2003;38:951–966.
2. Hermans PH, Bredée HL. Zur Kenntnis der Filtrationsgesetze. *Rec Trav Chim des Pays-Bas*. 1935;54:680–700.
3. Hermans PH, Bredée HL. Principles of the mathematical treatment of constant-pressure filtration. *J Soc Chem Ind*. 1936;55T:1–4.
4. Grace HP. Structure and performance of filter media. II. Performance of filter media in liquid service. *AIChE J*. 1956;2:316–336.
5. Shirato M, Aragaki T, Iritani E. Blocking filtration laws for filtration of power-law non-Newtonian fluids. *J Chem Eng Jpn*. 1979;12:162–164.
6. Hermia J. Constant pressure blocking filtration laws—application to power-law non-Newtonian fluids. *Trans IChemE*. 1982;60:183–187.
7. Iritani E, Sumi H, Murase T. Analysis of filtration rate in clarification filtration of power-law non-Newtonian fluids-solids mixtures under constant pressure by stochastic model. *J Chem Eng Jpn*. 1991;24:581–586.
8. Kim KJ, Chen V, Fane AG. Ultrafiltration of colloidal silver particles: flux, rejection, and fouling. *J Colloid Interface Sci*. 1993;155:347–359.
9. Huang L, Morrissey MT. Fouling of membranes during microfiltration of surimi wash water: roles of pore blocking and surface cake formation. *J Membr Sci*. 1998;144:113–123.
10. Blanpain-Avet P, Filaudeau L, Lalande M. Investigation of mechanisms governing membrane fouling and protein rejection in the sterile microfiltration of beer with an organic membrane. *Trans IChemE Part C Food Bioprod Process*. 1999;77:75–89.
11. Purkait MK, Bhattacharya PK, De S. Membrane filtration of leather plant effluent: Flux decline mechanism. *J Membr Sci*. 2005;258:85–96.
12. Ho CC, Zydney AL. A combined pore blockage and cake filtration model for protein fouling during microfiltration. *J Colloid Interface Sci*. 2000;232:389–399.
13. Bolton G, LaCasse D, Kuriyel R. Combined models of membrane fouling: development and application to microfiltration and ultrafiltration of biological fluids. *J Membr Sci*. 2006;277:75–84.
14. Duclos-Orsello C, Li W, Ho CC. A three mechanism model to describe fouling of microfiltration membranes. *J Membr Sci*. 2006;280:856–866.
15. Lee DJ. Filter medium clogging during cake filtration. *AIChE J*. 1997;43:273–276.
16. Iritani E, Mukai Y, Furuta M, Kawakami T, Katagiri N. Blocking resistance of membrane during cake filtration of dilute suspensions. *AIChE J*. 2005;51:2609–2614.
17. Bowen WR, Calvo JI, Hernández A. A steps of membrane blocking in flux decline during protein microfiltration. *J Membr Sci*. 1995;101:153–165.
18. Iritani E, Mukai Y, Tanaka Y, Murase T. Flux decline behavior in dead-end microfiltration of protein solutions. *J Membr Sci*. 1995;103:181–191.
19. Hwang KJ, Liao CY, Tung KL. Analysis of particle fouling during microfiltration by use of blocking models. *J Membr Sci*. 2007;287:287–293.
20. Iritani E, Katagiri N, Sugiyama Y, Yagishita K. Analysis of flux decline behaviors in filtration of very dilute suspensions. *AIChE J*. 2007;53:2275–2283.
21. Bolton GR, LaCasse D, Lazzara MJ, Kuriyel R. The fiber-coating model of biopharmaceutical depth filtration. *AIChE J*. 2005;51:2978–2987.
22. Ives KJ, Pienvichitr V. Kinetics of the filtration of dilute suspension. *Chem Eng Sci*. 1965;20:965–973.
23. Tien C, Payatakes AC. Advances in deep bed filtration. *AIChE J*. 1979;25:737–759.

24. Choo CU, Tien C. Simulation of hydrosol deposition in granular media. *AIChE J*. 1995;41:1426–1442.
25. Rodgers VGJ, Oppenheim SF, Datta R. Correlation of permeability and solute uptake in membrane of arbitrary pore morphology. *AIChE J*. 1995;41:1826–1829.
26. Iritani E, Tachi S, Murase T. Influence of protein adsorption on flow resistance of microfiltration membrane. *Colloids Surfaces A Physicochem Eng Aspects*. 1994;89:15–22.
27. Hwang KJ, Chou FY, Tung KL. Effects of operating conditions on the performance of cross-flow microfiltration of fine particle/protein binary suspension. *J Membr Sci*. 2006;274:183–191.
28. Polyakov YS. Depth filtration approach to the theory of standard blocking: Prediction of membrane permeation rate and selectivity. *J Membr Sci*. 2008;322:81–90.
29. Carman PC. Fluid flow through granular beds. *Trans IChemE*. 1937;15S:32–48.
30. Bowen WR, Gan Q. Microfiltration of protein solutions at thin film composite membranes. *J Membr Sci*. 1993;80:165–173.
31. Hlavacek M, Bouchet F. Constant flowrate blocking laws and an example of their application to dead-end microfiltration of protein solutions. *J Membr Sci*. 1993;82:285–295.
32. Blanpain P, Hermia J, Lenoël M. Mechanisms governing permeate flux and protein rejection in the microfiltration of beer with cyclopore membrane. *J Membr Sci*. 1993;84:37–51.
33. Hwang KJ, Chiu HS. Influence of membrane type on filtration characteristics and protein rejection in crossflow microfiltration. *Filtration*. 2008;8:317–322.
34. Iritani E, Katagiri N, Sengoku T, Yoo KM, Kawasaki K, Matsuda A. Flux decline behaviors in dead-end microfiltration of activated sludge and its supernatant. *J Membr Sci*. 2007;300:36–44.
35. Iritani E, Nagaoka H, Katagiri K. Determination of filtration characteristics of yeast suspension based upon multistage reduction in cake surface area under step-up pressure conditions. *Sep Purif Technol*. 2008;63:379–385.

Manuscript received Feb. 9, 2009, revision received Aug. 7, 2009, and final revision received Oct. 8, 2009.